RSC Advances

PAPER

View Article Online
View Journal | View Issue

Cite this: *RSC Adv.*, 2024, **14**, 9781

Luminescence turn-on sensor for the selective detection of trace water and methanol based on a Zn(II) coordination polymer with 2,5-dihydroxyterephthalate†

Jitti Suebphanpho and Jaursup Boonmak *

A highly selective detection of trace water in organic solvents is urgently required for the chemical industry. In this work, the simple sonochemical method was used for producing a luminescent sensor, $[Zn(H_2dhtp)(2,2'\text{-bpy})(H_2O)]_n$ (**Zn-CP**) (H_2dhtp^{2-} = 2,5-dihydroxyterephthalate and 2,2′-bpy = 2,2′-bipyridine). **Zn-CP** exhibits reversible thermally-induced and methanol-mediated structural transformation. Importantly, **Zn-CP** has exceptional water sensing performance in both dry methanol and dry ethanol, with high selectivity, wide linear ranges, and a low limit of detection (LOD) of 0.08% (v/v). Upon the incremental addition of water, the luminescent intensities enhanced and shifted, along with the emission color changing from green to greenish yellow. In addition, **Zn-CP** can detect methanol selectively through turn-on luminescence intensity with LODs of 0.28, 0.52, and 0.35% (v/v) in dry ethanol, dry *n*-propanol, and dry *n*-butanol, respectively. The excited-state proton transfer of linker H_2dhtp^{2-} *via* enol–keto tautomerism and collaboration with structural transformation could be attributed to the sensing mechanism.

Received 19th January 2024
Accepted 16th March 2024

DOI: 10.1039/d4ra00500g

rsc.li/rsc-advances

1 Introduction

Over the past few decades, research in the field of coordination polymers (CPs) has received a great deal of attention because of their broad potential applications, such as heterogeneous catalysis, gas storage and separation, sensing, and magnetism.[1–3] The building blocks of CPs are constructed by metal ions and organic ligands, and their physical properties can be directly tuned by the selection of metal ions and organic ligands on a coordination assembly.[4–6] The reversible structural transformation with chromotropism of CPs has been attracting great attention due to their vital importance for application in thermo-sensors, chemical sensors, optical sensors, color indicators, and molecular switches.[7–10] There are three main categories of structural changes: solid-state, solution-based, and solvent-mediated.[11–13] The solvent-mediated structural transformation in CPs is rarely reported, owing to the dissolve-recrystallize process of crystallization, which commonly induces significant changes in their structures and properties.[14,15]

Nowadays, water is considered a contaminant and impurity in dry organic products, food inspection, environmental monitoring, and pharmaceutical manufacturing.[16–20] Trace water influences not only the yield of chemicals and drugs but also their activity and application.[21] Up until now, the traditional Karl Fischer titration method and gas chromatography have been used for monitoring water, but these methods have certain limitations, involving the requirements of specialized instruments, well-trained personnel, and time-consuming processes.[22,23] Therefore, the development of sensors for detecting water in organic products with simple operation, fast response, and low detection limits is highly desired.[23,24] On the other hand, another important analyte is methanol, which is easily mixed into other alcohol solvents, especially ethanol, due to its analogous physical and chemical properties.[25,26] Ethanol is an essential ingredient that is widely used in a variety of industries, including the food and chemical industries. When methanol is mixed with ethanol, the cost of producing ethanol is reduced. Furthermore, methanol is an alcohol that is toxic to mammals; consuming the compound will result in headaches, vomiting, blindness, or worse, representing one of the world's major risks to food safety.[27,28] Therefore, the detection of methanol in alcohol solvents is of great significance and required.

It is well known that the excited-state intramolecular proton transfer (ESIPT) process of the organic ligand can greatly improve the sensitivity and selectivity of CPs sensing probes.

Materials Chemistry Research Center, Department of Chemistry, Faculty of Science, Khon Kaen University, Khon Kaen 40002, Thailand. E-mail: jaursup@kku.ac.th

† Electronic supplementary information (ESI) available: Figures for crystal structures, FT-IR spectra, PXRD patterns of **Zn-CP** and **Zn-CP-II**, TG curve of **Zn-CP**, PL spectra and CIE diagrams and other data. See DOI: https://doi.org/10.1039/d4ra00500g

Upon being stimulated by light, the ESIPT process can generate rapid intramolecular proton transfer between the hydrogen bond donors (–OH and –NH_2) and hydrogen bond acceptors (=N– and –C=O) of the molecular structure *via* tautomerism from the excited enol form to keto form.[29–31] From this viewpoint, 2,5-dihydroxyterephthalate (H_2dhtp^{2-}) was selected to construct CPs for the sensing probe. The H_2dhtp^{2-} ligand consists of two carboxylate groups for constructing stable CPs and realizing a high-efficiency ESIPT process that originates from weak intramolecular H-bonds between carboxylate and hydroxyl groups.[32] When adding the target molecule, it might interact with the –OH groups of H_2dhtp^{2-} and affect the enol–keto tautomerism during the ESIPT process, which suggests that luminescence emission peak position and intensity change after detection.[22,33] Out of the above-mentioned considerations, we successfully prepared $[Zn(H_2dhtp)(2,2'\text{-bpy})(H_2O)]_n$ (**Zn-CP**) (H_2dhtp^{2-} = 2,5-dihydroxyterephthalate and 2,2′-bpy = 2,2′-bipyridine) by the simple sonochemical method. **Zn-CP** presents a zigzag chain coordination polymer with an abundance of free hydroxy groups. The 1D zigzag chain structure of **Zn-CP** changes to 2D-layer **Zn-CP-II** by heating or soaking in methanol with chromotropism through the dehydration process. The luminescence properties of **Zn-CP** and **Zn-CP-II** in solid-state and suspension were studied. Furthermore, **Zn-CP** and **Zn-CP-II** can be applied for low water detection in dry methanol and dry ethanol with wide water detection ranges through the ESIPT mechanism, which produces enhanced and shifted emission spectra. In addition, by turning on luminescence intensity with low detection limits, **Zn-CP** is able to detect and discriminate methanol from a range of aliphatic alcohols.

2 Experimental section

2.1 Materials and methods

All chemicals and reagents were commercially available and used without further purification. FT-IR spectra were recorded over the range 4000–600 cm^{-1}, using a Bruker Tensor 27 Attenuated Total Reflectance Fourier Transform Infrared (ATR-FTIR) spectrophotometer. Powder X-ray diffraction (PXRD) patterns were obtained from 5° to 50° at a speed of 0.5 s per step on EMPYREAN PANALYTICAL using monochromatic CuKα radiation at room temperature. Thermogravimetric analyses (TGA) were measured using a TG-DTA 2010S MAC thermal analyzer under an N_2 atmosphere at a heating rate of 10 °C min^{-1} and a temperature range of 35–700 °C. The sonicator used in this study was an Elmasonic S30H (maximum 280 W at 50 Hz). The luminescence spectra were obtained by using a Shimadzu RF-6000 spectrofluorometer with a continuous Xe lamp at room temperature.

2.2 Preparation of $[Zn(H_2dhtp)(2,2'\text{-bpy})(H_2O)]_n$ (Zn-CP)

The synthesis of **Zn-CP** in this work was developed using the simple sonochemical method rather than the previously reported solvothermal reaction at 60 °C for 4 days.[34] Sodium acetate was used as a modulator in order to control the particle size of the product. $Zn(NO_3)_2 \cdot 6H_2O$ 0.2 mmol (56 mg), H_4dhtp 0.2 mmol (40 mg), 2,2′-bpy 0.2 mmol (31 mg), sodium acetate 0.2 mmol (54 mg), and NaOH 0.4 mmol (16 mg) were dissolved in 10 mL of a mixed solvent of water/ethanol (1 : 1 v/v). The mixture was sonicated for 30 min at room temperature. After the sonication process, the yellow powder of **Zn-CP** was obtained. Then, the product was centrifuged, and washed several times with water, and dried overnight at 70 °C. Yield: (78% based on Zn(II) salt). FT-IR (ATR, cm^{-1}) 3194(m), 1597(s), 1490(m), 1475(m), 1428(s), 1321(s), 1238(s), 1062(w), 1021(w), 804(m), 754(s).

2.3 Preparation of $[Zn(H_2dhtp)(2,2'\text{-bpy})]_n$ (Zn-CP-II)

The yellow powder of **Zn-CP** was heated at 140 °C for 3 hours, and then the white powder of **Zn-CP-II** was obtained. FT-IR (ATR, cm^{-1}) 3184(m), 1598(s), 1472(m), 1440(s), 1380(m), 1361(m), 1109(m), 1024(m), 866(m), 789(s), 760(s).

2.4 Water sensing experiment

To carry out the luminescent detection for water, 10 mg of the ground **Zn-CP** or **Zn-CP-II** was added to 100 mL of dry methanol or dry ethanol. After that, the mixture solution was sonicated at room temperature for 30 min, and a suspension of **Zn-CP** or **Zn-CP-II** in a methanolic or ethanolic solution was obtained. Then, 4 mL of the **Zn-CP** or **Zn-CP-II** suspension was pipetted into a 5 mL volumetric flask. After that, a different water level from 0.5 to 20% (v/v) was added. The volume of the suspension containing water was adjusted to 5 mL with dry methanol or dry ethanol, giving the different concentrations of water in the **Zn-CP** or **Zn-CP-II** luminescent probe. After that, this suspension was transferred to a quartz cuvette, followed by monitoring emission intensity upon excitation at 360 nm.

2.5 Methanol sensing experiment

10 mg of **Zn-CP** was added to 100 mL of dry ethanol, then it was sonicated for 30 min. After that, the suspension of **Zn-CP** in an ethanolic solution was obtained. The experiment was performed by the incremental addition of methanol to 5 mL of ethanolic suspension of **Zn-CP** in 10 mL of a volumetric flask to make the final content of methanol in the range of 5–50% (v/v). After that, the luminescence intensity was measured by exciting at 360 nm. Furthermore, the methanol sensing of **Zn-CP** in dry *n*-propanol or dry *n*-butanol can be carried out in the same way, but instead of dry ethanol to dry *n*-propanol or dry *n*-butanol.

3 Results and discussion

3.1 Structural characterization of Zn-CP and Zn-CP-II

A **Zn-CP** was prepared by the simple sonochemical method instead of the solvothermal method previously reported.[34] The sonochemical reaction serves to facilitate fast preparation and reduce energy consumption such as pressure or high-temperature heating. The powder X-ray diffraction (PXRD) pattern of **Zn-CP** matches well with the reported structural phase (Fig. S1†), suggesting that they are isostructural structures.[34] The structure of **Zn-CP** presents a 3D supramolecular framework. Each Zn(II) center is five-coordinated and consists of two oxygen atoms from different H_2dhtp^{2-} ligands, two nitrogen atoms from

a chelating 2,2′-bpy ligand, and one oxygen atom from a water molecule (Fig. S2†). Monodentate H_2dhtp^{2-} ligands bridge two Zn(II) to form a 1D zigzag chain. For the packing structure of **Zn-CP**, each 1D zigzag chain is linked together through π–π interaction between the aromatic ring of H_2dhtp^{2-} and the pyridine ring of 2,2′-bpy along the *c*-axis, generating a 2D-layer structure with free hydroxy group of H_2dhtp^{2-}, which is the active site for the ESIPT process (Fig. S3†). The adjacent 2D layers of **Zn-CP** are assembled to the 3D supramolecular framework by hydrogen bonding along the *b*-axis between the hydrogen atom of the coordinated water molecule and the uncoordinated oxygen atom of the carboxyl group in different units (Fig. S4†). The TGA analysis of **Zn-CP** displays a weight loss of 4.01% at temperatures around 100 °C that indicates the release of a coordinated water molecule (anal. Calc., 4.13%). In addition, the **Zn-CP** shows high thermal stability up to 300 °C, and then the organic ligands were decomposed (Fig. S8†).

Zn-CP-II was prepared by heating **Zn-CP** at 140 °C for 3 h. The PXRD pattern of as-synthesized **Zn-CP-II** is well matched with that of the simulated pattern of reported single crystal data,[34] confirming the identical crystalline phase purity (Fig. S1†).The crystal structure of **Zn-CP-II** displays a 3D supramolecular framework. The Zn(II) center is five-coordinated and surrounded by three oxygen atoms of carboxylate groups from different H_2dhtp^{2-} ligands and two nitrogen atoms from a chelating 2,2′-bpy ligand (Fig. S5†). The carboxylate groups of H_2dhtp^{2-} ligands show the bidentate and monodentate bridging modes for connecting with four and two Zn(II) centers, respectively, which generate the 2D layer of **Zn-CP-II** along the *bc* plane (Fig. S6†). For the packing motif of **Zn-CP-II**, each 2D layer is connected through intramolecular hydrogen bonds between different hydroxyl groups of different H_2dhtp^{2-} ligands and hydrogen bonds between hydroxyl groups and carboxylate groups of H_2dhtp^{2-} ligands. Moreover, each 2D-layer is packed by intramolecular π–π interactions between pyridyl rings of different 2,2′-bpy, as shown in Fig. S6.† Furthermore, the adjacent 2D layers of **Zn-CP-II** are assembled to the 3D supramolecular framework through interlayer C–H···π interactions among the hydrogen atoms from the adjacent 2,2′-bpy units and benzene rings of H_2dhtp^{2-} ligands (Fig. S7†).

3.2 Reversible thermal- and methanol-induced structural transformation in Zn-CP

According to the TGA results, upon heating **Zn-CP** at 140 °C for 3 h, the coordinated water molecule in **Zn-CP** was removed to be

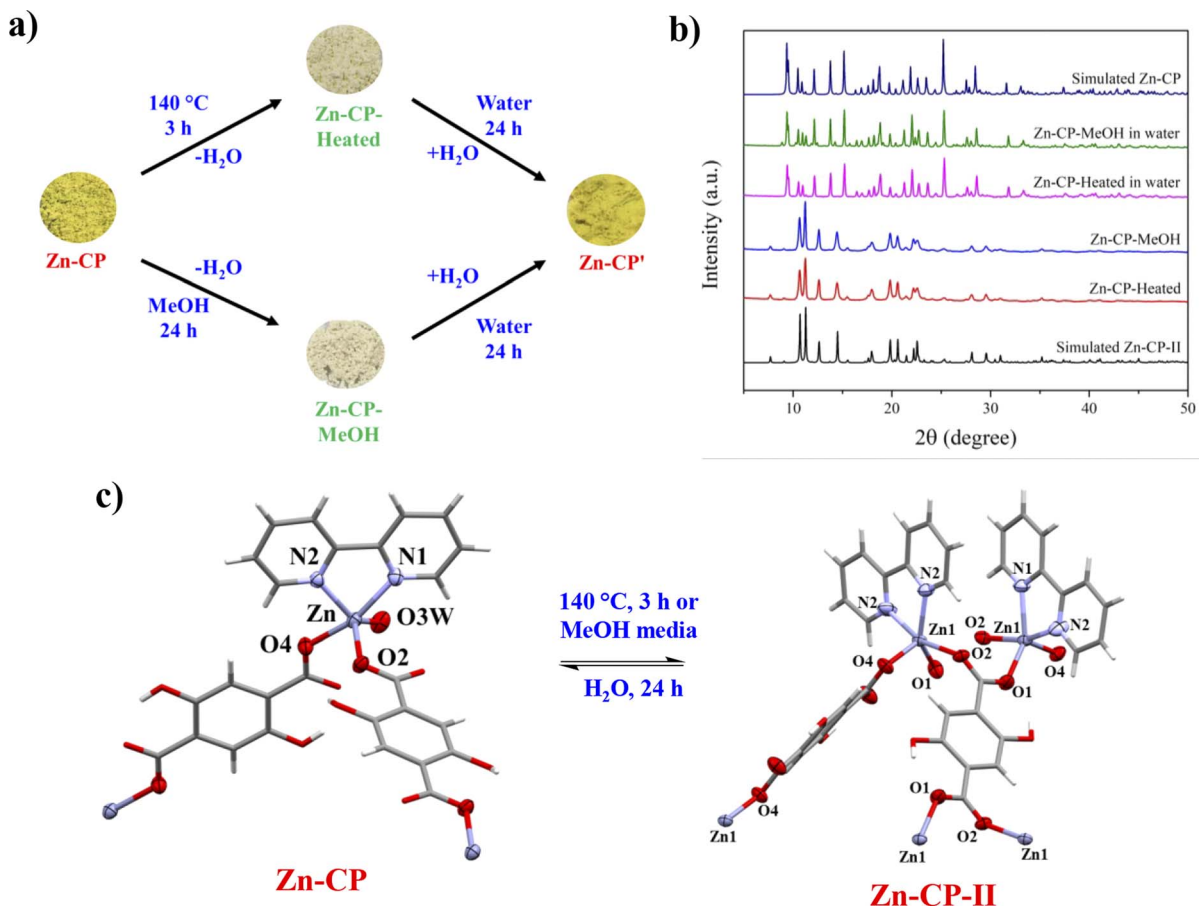

Fig. 1 (a) Diagram of reversible dehydration and rehydration processes with color change of **Zn-CP** induced by thermal and methanol media. (b) PXRD patterns of **Zn-CP**, **Zn-CP-II**, **Zn-CP-Heated** (**Zn-CP** was heated at 140 °C), **Zn-CP-MeOH** (**Zn-CP** was soaked in methanol), and its rehydrated form after soaking in water (**Zn-CP-Heated** and **Zn-CP-MeOH** in water). (c) A view of the reversible structural transformation of **Zn-CP** and **Zn-CP-II** induced by thermal and methanol.

an activated form (denoted as **Zn-CP-Heated**), and the color was also changed from yellow to white (Fig. 1a). The reversible structural transformation of **Zn-CP** relating to its dehydration and rehydration processes was monitored by FTIR and PXRD techniques. The FTIR spectrum of **Zn-CP-Heated** shows that the $\nu(OH)_{water}$ at 3031 cm^{-1} clearly disappears compared with the original **Zn-CP** (Fig. S9†). In addition, the PXRD patterns of **Zn-CP-Heated** are different from **Zn-CP**, indicating the structural transformation after the dehydration process. Also, the PXRD pattern of **Zn-CP-Heated** matched the reported structure of [Zn(H_2dhtp)(2,2′-bpy)] (**Zn-CP-II**).[34]

To examine the solvent-mediated structural transformation, 50 mg of the ground **Zn-CP** was soaked in 14 different solvents at room temperature. Interestingly, the color of **Zn-CP** was changed from yellow to white only in the methanol media, as shown in Fig. 1a (denoted as **Zn-CP-MeOH**). In contrast, **Zn-CP** shows no significant color change in other solvents after soaking for 24 h (Fig. 2a). The PXRD pattern of **Zn-CP-MeOH** shows the same diffraction pattern as the simulated **Zn-CP-II**, confirming that the structural changed from the 1D chain of **Zn-CP** to the 2D layer of **Zn-CP-II**. Time-dependent PXRD patterns of **Zn-CP** in methanol were also investigated. When **Zn-CP** is soaked in methanol for 5–20 min, the majority of the products are the same as **Zn-CP**, which is greater than **Zn-CP-II**. Nevertheless, some diffraction peaks of **Zn-CP-II** at $2\theta = 11.2°$, 12.6°, and 14.5° were obtained, which indicate the mixed phases between **Zn-CP** and **Zn-CP-II**. After soaking in methanol for more than 30 min, some characteristic diffraction peaks of **Zn-CP** at $2\theta = 9.3°$, 9.5°, 10.9°, 12.1°, 13.8°, 15.1°, 25.2°, 28.5°, and 31.6° disappeared. Also, only the appearance of diffraction peaks of **Zn-CP-II** is obtained after soaking in methanol for 60 min (Fig. 2b and c), indicating that the structure completely changed from **Zn-CP** to **Zn-CP-II**. It is worth mentioning that **Zn-CP** does not exhibit a change in color or structural transformation upon contact with other common organic solvents (Fig. 2a), which corresponds to the PXRD patterns (Fig. S10†). Therefore, the structural transformation with chromotropism is selective toward methanol over other solvents. The structural transformation mechanism could be determined by the size[35] and hydrogen bonding ability of methanol, which are confirmed by Kamlet–Taft parameters[36] (Table S1†). Methanol has a tiny size and high hydrogen bond donor (α) and acceptor (β) parameters; thus, it is easily accessible to the lattice structure of **Zn-CP**. Also, the coordinated water molecule of **Zn-CP** has the highest hydrogen bond donor parameter, which generates strong hydrogen bonds between them.[37] Due to the strong hydrogen bonding, the coordinated water molecule can be removed from the coordination sphere, which indicates the methanol-mediated structural transformation. Furthermore, **Zn-CP-Heated** and **Zn-CP-MeOH** can be restored to the original crystalline phase of **Zn-CP** after being soaked in water at room temperature for 24 h. The rehydrated crystalline solid after soaking in water for 24 h shows the same PXRD patterns as the original phase of **Zn-CP** (Fig. 1b). Also, the color was returned to that of the original one, as shown in Fig. 1a. These results confirm the reversible thermal-induced and MeOH-mediated structural phase transformation with chromotropism in **Zn-CP**. It is worth mentioning that **Zn-CP-II** (both **Zn-CP-Heated** and **Zn-CP-MeOH**) cannot return to **Zn-CP** after exposure to air for a month, implying the high stability of **Zn-CP-II** in air.

3.3 Luminescence properties of Zn-CP and Zn-CP-II

The solid-state luminescence properties of H_4dhtp, 2,2′-bpy, **Zn-CP**, and **Zn-CP-II** were investigated (Fig. 3). Upon excitation at

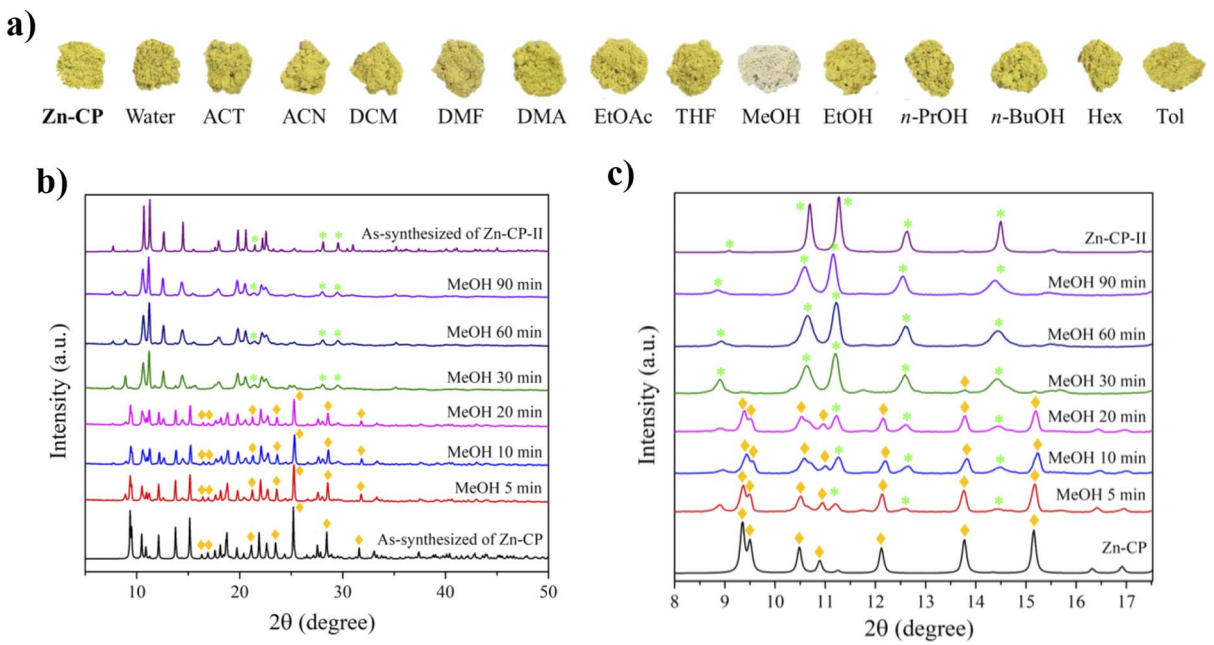

Fig. 2 (a) Photographs of **Zn-CP** after soaking in different solvents. (b) Time-dependent and (c) amplified time-dependent PXRD patterns at $2\theta =$ 8–18° of **Zn-CP** in methanol. The green star and orange diamond symbols represent characteristic diffraction peaks for **Zn-CP** and **Zn-CP-II**, respectively.

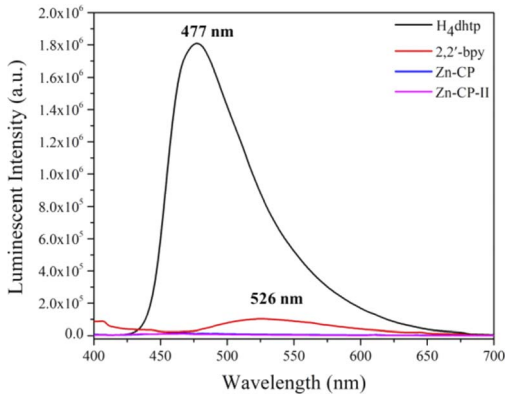

Fig. 3 Solid-state PL spectra of free H_4dhtp, 2,2′-bpy, **Zn-CP**, and **Zn-CP-II** upon excitation at 360 nm.

360 nm, the luminescence intensity of free H_4dhtp and 2,2′-bpy ligands is observed at 477 and 526 nm, respectively, showing the blue and white colors under UV light that originate from the π* to *n* or π* to π electronic transition.[35,37] In contrast, **Zn-CP** and **Zn-CP-II** show the quenching luminescent emission in solid-state when compared with the free ligands, and other CPs containing H_4dhtp ligand normally show strong emission in solid-state, as shown in Table S2.† The quenching phenomenon in **Zn-CP** and **Zn-CP-II** is unique because the H_4dhtp ligand is a strong luminescent organic chromophore that can be changed from enol to keto *via* excited-state intramolecular proton transfer (ESIPT) between hydrogen atoms from the hydroxy group to the carboxylate group after being excited by UV-light. The weak luminescent intensity of **Zn-CP** could be attributed to (i) the loss of energy from the vibration of the phenolic ligand in the excited state,[38,39] (ii) the molecular aggregation and characteristics of molecular stacking. Generally, J-aggregation (slip-stacking/head-to-tail interaction) enhances the fluorescence emission over H-aggregation (face-to-face interaction) for ESIPT.[40–42] The packing structure of **Zn-CP** and **Zn-CP-II** displayed intermolecular face-to-face interaction between rings of ligands in 1D chains and 2D layers (Fig. S3 and S6†), which originated the aggregation-caused quenching (ACQ) effect. (iii) The ligand-to-ligand charge transfer (LLCT) in **Zn-CP**. The previous study used DFT to calculate the molecular orbital simulation of $[Zn(bpy)(dhtp)_{0.5}]_n$.[43] The composition of this compound is the same as that of **Zn-CP** and **Zn-CP-II**, but with different packing structures and coordination modes of $dhtp^{4-}$. The HOMO is provided by the C and O atoms of the $dhtp^{4-}$ when emitting light energy, it transfers to the 2,2′-bpy on the LUMO, which is the LLCT process causing the quenching luminescence intensity.[43]

The suspension of **Zn-CP** and **Zn-CP-II** showed strong emission in water, methanol, DMF, and DMA, as shown in Fig. 4. In strong polar protic solvents like water, **Zn-CP** and **Zn-CP-II** showed strong luminescence intensity at 537 nm with yellow emission. This phenomenon could be attributed to the intermolecular proton transfer process between water and proton in the hydroxyl group of H_2dhtp^{2-}. Other polar protic solvents such as MeOH, EtOH, *n*-propanol (*n*-PrOH), and *n*-butanol (*n*-BuOH), polar aprotic solvents such as acetone (ACT), acetonitrile (ACN), dichloromethane (DCM), dimethyl formamide (DMF), dimethylacetamide (DMA), ethyl acetate (EtOAc), tetrahydrofuran (THF), and non-polar solvents such as hexane (Hex) and toluene (Tol) show the green luminescence color at 503, 502, 507, and 510 nm in MeOH, EtOH, DMF, and DMA, respectively, depending on solvent polarity.[44,45] **Zn-CP** and **Zn-CP-II** contain hydroxyl groups in H_2dhtp^{2-} thus methanol or ethanol can easily interact with hydroxyl groups due to their small size with high hydrogen bond donor and acceptor parameters. DMF and DMA suspensions display green emission due to their higher polarizability (Table S1†). Moreover, the high polarity of water can be more stabilized in the excited state than the ground state due to solvent relaxation, resulting in a decreased energy band gap and a red-shitted emission when compared to other solvents (Fig. 4b and c).

3.4 Water sensing of Zn-CP and Zn-CP-II

Based on the above results, the emission spectra of **Zn-CP** and **Zn-CP-II** in water suspensions show significantly red-shifted emission when compared to other solvents (Fig. 4b), so the utilization of **Zn-CP** and **Zn-CP-II** for trace amounts of water in dry methanol or dry ethanol was investigated. As shown in Fig. 5, the luminescence intensity upon adding water to the **Zn-CP** suspension was dramatically increased and red-shifted from 501 to 537 nm (≈35 nm) and 497 to 522 nm (≈25 nm) in dry methanol and dry ethanol, respectively (Fig. 5c and d). The luminescence color under the irradiation of a 365 nm UV lamp is switched from green to green-yellow (Fig. 5a and b), corresponding with the CIE diagram (Fig. S11†). The correlations between luminescence intensity and water contents are fitted, exhibiting good linear ranges at low water content 0–12% v/v with R^2 values of 0.999 and 0.995 in dry methanol and dry ethanol, respectively. The limit of detection (LOD) for a trace of water is determined by LOD = $3\sigma/S$ (σ is the standard deviation of the luminescence test for 10 blank solutions, and S is the slope of the linear equation curve); the LODs of water in both dry methanol and dry ethanol were calculated to be as low as 0.08% v/v (Fig. 5e and f). Moreover, the luminescence response of **Zn-CP-II** toward water in dry methanol and dry ethanol was examined under the same conditions as in **Zn-CP** (Fig. S14†). It was revealed that the luminescence intensity of **Zn-CP-II** was gradually raised and red-shifted from 502 to 536 nm (≈35 nm) and 497 to 511 nm (≈14 nm) with increasing water contents in dry methanol and dry ethanol, respectively. The luminescence color has a striking transition from blue to green-yellow and blue to green in dry methanol and dry ethanol, respectively, which is beneficial for visual detection by the naked eye under a 365 nm UV lamp and confirmed by CIE diagrams (Fig. S15†). A good linear relationship between luminescence intensity and water contents was obtained in 0–20 and 1–10% v/v with R^2 = 0.999 in both dry methanol and dry ethanol. The LODs of water in dry methanol and dry ethanol in **Zn-CP-II** suspension were calculated to be 0.05 and 0.04% v/v, respectively. The LOD values for water in dry methanol and dry ethanol of **Zn-CP** and **Zn-CP-II** are comparable to other CPs, as shown in Table S3,†

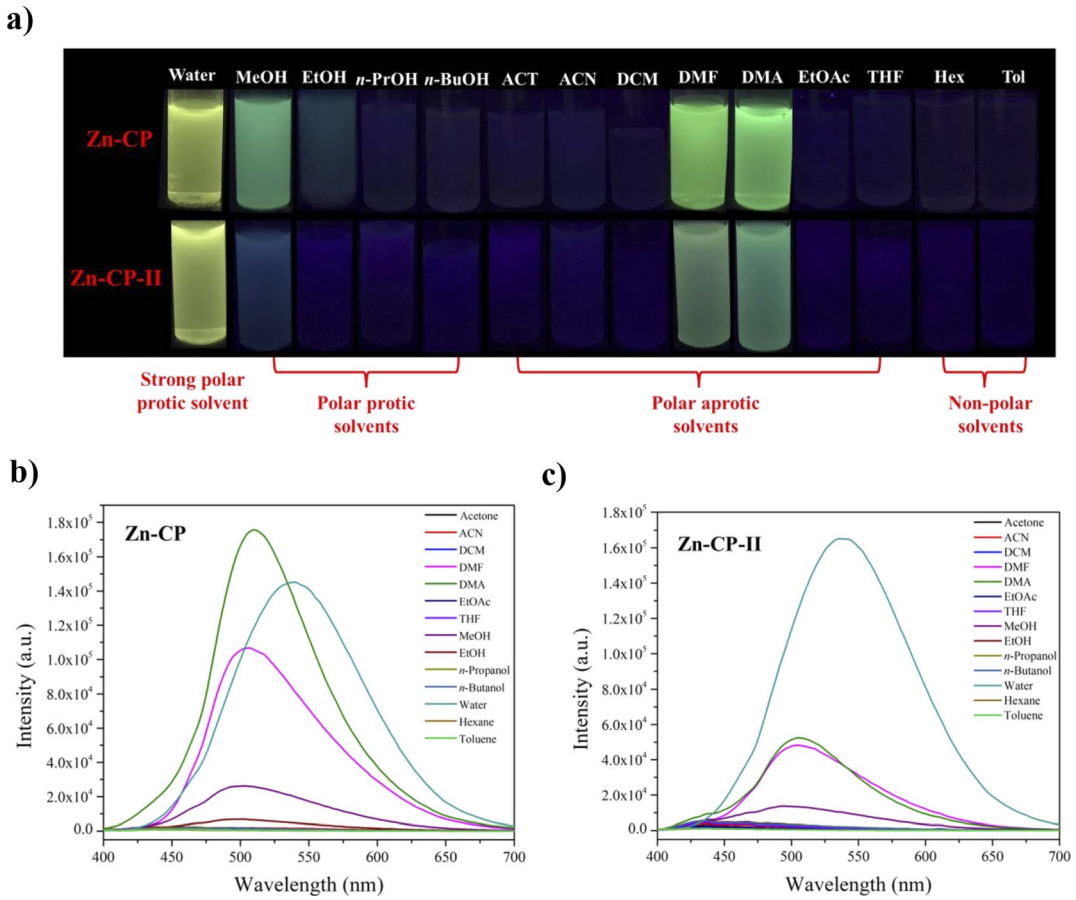

Fig. 4 (a) Photographs of Zn-CP (top) and Zn-CP-II (bottom) in different dry solvents under UV irradiation. Emission PL spectra of (b) Zn-CP and (c) Zn-CP-II in different dry solvents at $\lambda_{ex} = 360$ nm.

and lower than those found in AEHC (hydrated ethyl alcohol fuel: 0.8 in China, 1.0% in the US, and 4.9% in Brazil).[46] The water sensing mechanism for **Zn-CP** could be explained as follows: (i) when water was added to a dry methanol or dry ethanol suspension of **Zn-CP**, the suspension became more polar, increasing the luminescence intensity; (ii) water molecules may acquire a proton from the hydroxy groups of the H_2dhtp^{2-} ligand, generating H_3O^+ along with the intermolecular proton transfer process (Fig. 5g), resulting in the red-shifted emission.[21,22,47] Additionally, the stability of **Zn-CP** after water sensing can be confirmed by FTIR and PXRD techniques. The FTIR spectra and PXRD patterns of **Zn-CP** display identical patterns to those of the pristine **Zn-CP** (Fig. S12 and S13†), implying that the structure did not change from **Zn-CP** to **Zn-CP-II** during the water sensing process. In the case of **Zn-CP-II**, the FTIR spectra show some characteristic peaks of **Zn-CP** after water sensing (Fig. S16†) and the PXRD pattern of **Zn-CP-II** after water sensing in dry methanol or dry ethanol shows mixed crystalline phases between **Zn-CP** and **Zn-CP-II** (Fig. S17†), implying the structural transformation process from **Zn-CP-II** to **Zn-CP**. The water molecules can be coordinated with Zn(II) centers, which corresponds to a change from a 2D-layer of **Zn-CP-II** to a 1D-zigzag chain of **Zn-CP**. The water sensing mechanism of **Zn-CP-II** can be explained based on the following considerations: (i) at low water content, the majority phase is **Zn-CP-II**, which is confirmed by its characteristic emission color (blue-green emission color, Fig. S14a†); (ii) at high water content, the bright-green emission color was obtained, confirming the majority phase of **Zn-CP**. Moreover, the luminescence intensity increased, and red-shifted emission could be caused by an intermolecular proton transfer between the hydroxy and water molecules. From these results, **Zn-CP** and **Zn-CP-II** show not only facile water detection without a complicated method but also are very cost-effective and environmentally friendly.

3.5 MeOH sensing of Zn-CP

When comparing the luminescence intensity at the maximum peak of the **Zn-CP** probe in four different alcohols (Fig. 4b), methanol has the highest luminescence intensity (Table S4†). Thus, we further explored the performance of the **Zn-CP** probe in detecting methanol in various dry alcohol suspensions. Upon adding different methanol levels (0–50% v/v) to dry ethanol, the luminescence intensity gradually increased (Fig. 6b). The luminescence color under the irradiation of a 365 nm UV lamp switches from blue to green, which can be easily observed. The correlation between the luminescence intensity and methanol contents (5–30% v/v) is fitted. The linear relationship is $Y =$

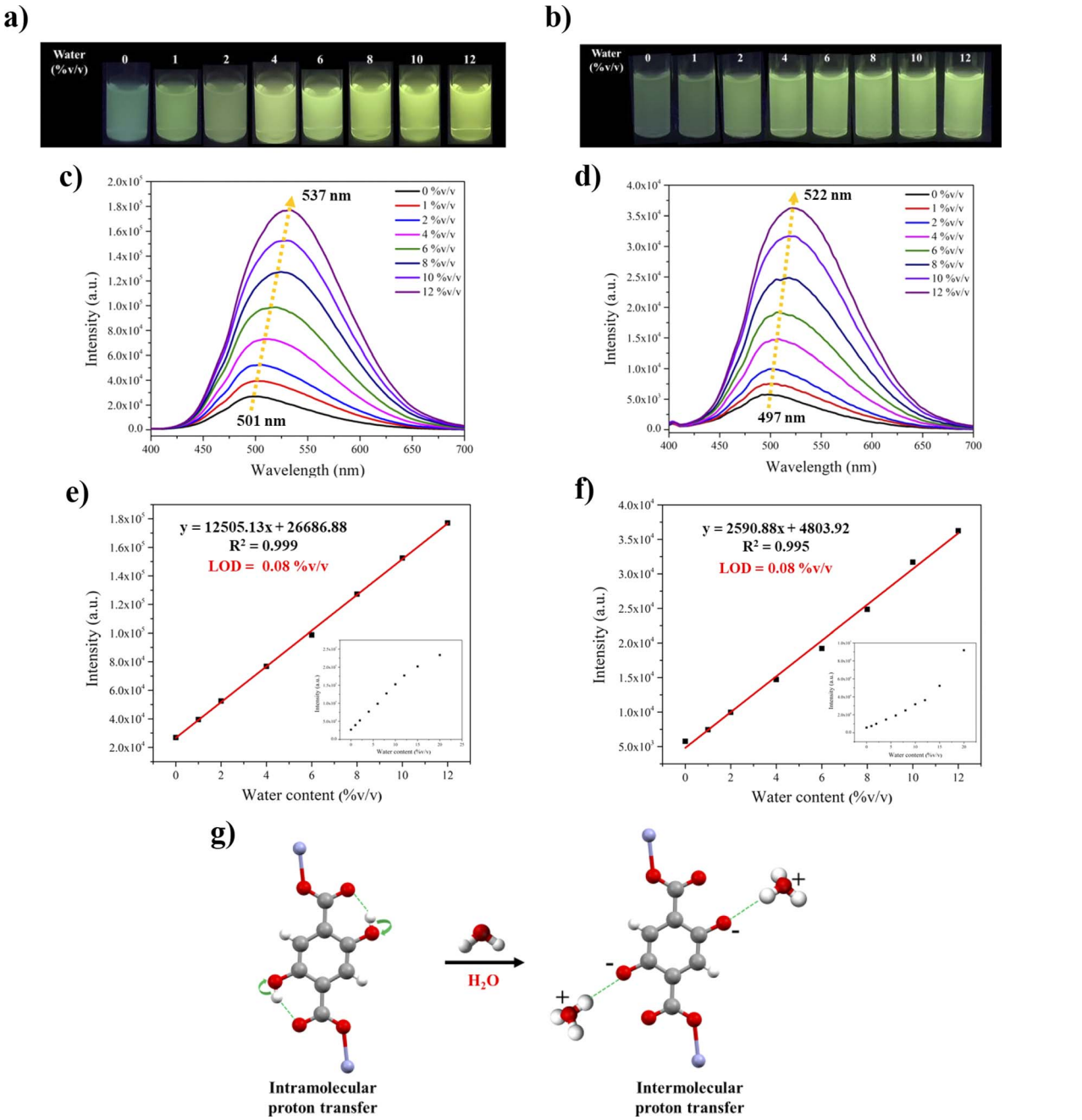

Fig. 5 Photographic images of the suspension of **Zn-CP** in (a) dry methanol and (b) dry ethanol with different water levels (0–12%). (c) and (d) Luminescence emission spectra of **Zn-CP** probe upon adding different contents of water to dry methanol and dry ethanol, respectively. (e) and (f) Linear relationship between the emission wavelength or luminescence intensity and water contents of **Zn-CP** probe in dry methanol and dry ethanol, respectively. The inset shows fluorescence intensity upon incremental addition of water 0–20% v/v. (g) The schematic represents the proposed water sensing mechanism of **Zn-CP**.

688.31X − 667.28, with the calibration curve R^2 = 0.999, implying a good linear relationship between the luminescence intensity and methanol content. The result shows that methanol in dry ethanol can be detected using the **Zn-CP** probe with a LOD value of 0.28% v/v (Fig. 6c). According to the excellent luminescence sensing performance of **Zn-CP** for detecting methanol in dry ethanol, its luminescence sensing behavior in other alcohols, such as dry *n*-propanol and dry *n*-butanol, was further investigated. The results of luminescence sensing are shown in Fig. S18 and 19.† The luminescence intensity increased with the increase in methanol content, showing a turn-on luminescence response (Fig. S18b and S19b†). The luminescence intensity and methanol content showed a good linear relationship with R^2 values of 0.996 and 0.998 and low LOD values of 0.52 and 0.35% v/v in dry *n*-propanol and dry *n*-butanol, respectively. The linear ranges and LODs are

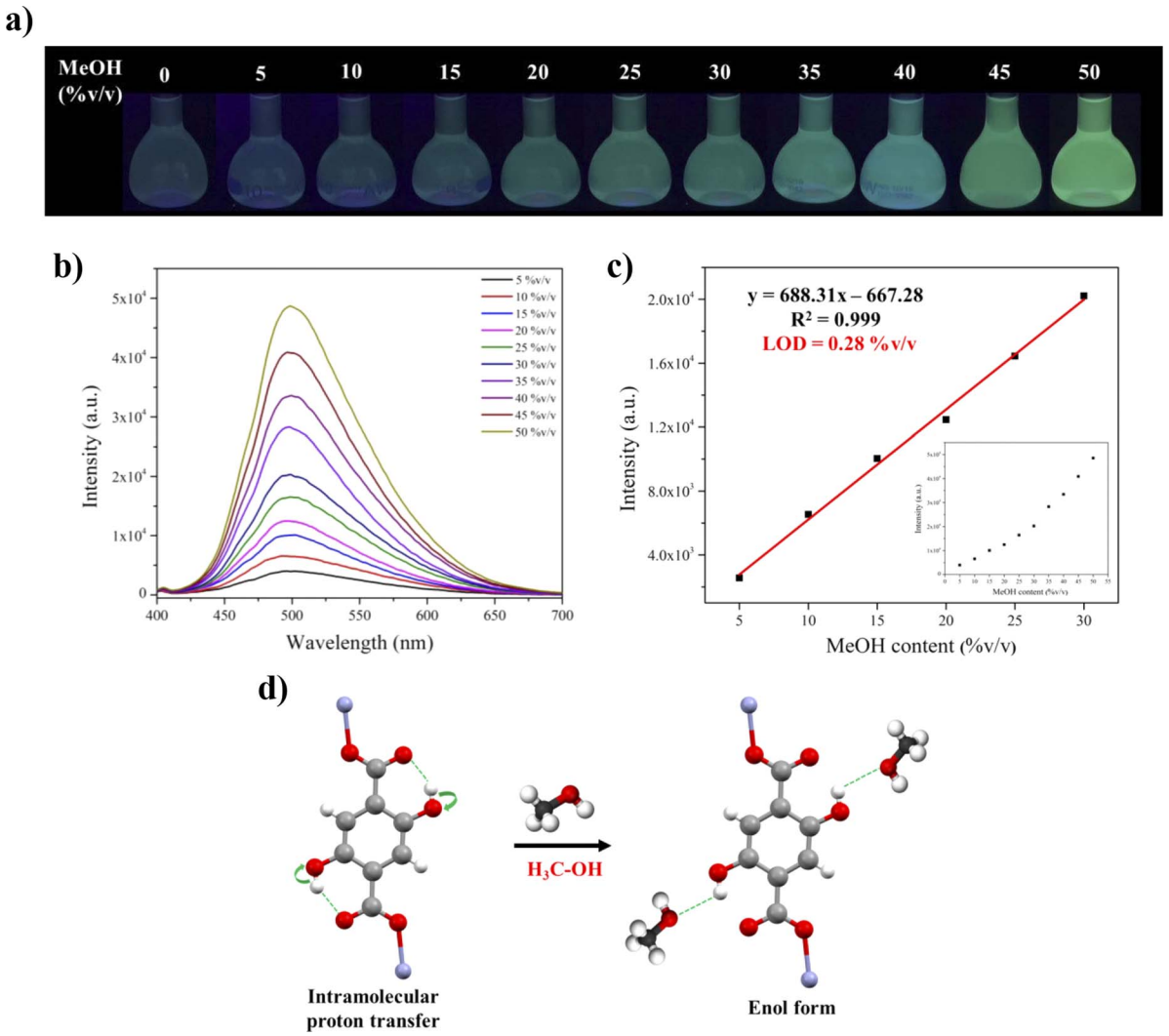

Fig. 6 (a) Photographic images of the suspension of Zn-CP in dry ethanol with different methanol levels (0–50% v/v). (b) Luminescence emission spectra of Zn-CP probe upon adding different amounts of methanol to dry ethanol. (c) Linear relationship between the luminescence intensity and methanol content of Zn-CP. (d) The schematic represents the proposed methanol sensing mechanism of Zn-CP.

summarized in Table S5,† which are comparable with the reported luminescence methanol sensors. These results prove that the **Zn-CP** probe can detect methanol in three common dry alcohol solvents with good linear ranges and low LODs. The sensing mechanism can be explained by the ESIPT process. Methanol is a small molecule with high polarizability when compared with ethanol, *n*-propanol, and *n*-butanol. Upon adding the methanol to the dry alcohol solvents, the methanol can easily interact with the hydroxyl group of H_2dhtp^{2-} in **Zn-CP**, implying that it reduces the O–H vibration energy and increases luminescence intensity with green emission.[35] This phenomenon effectively interrupts excited-state intramolecular proton transfer from the hydroxyl group and carboxylate group, showing the enol form in H_2dhtp^{2-} ligand,[22] as shown in Fig. 6d. Moreover, the PXRD pattern of **Zn-CP** after methanol sensing in dry ethanol shows mixed-phases of diffraction peaks between **Zn-CP** and **Zn-CP-II**, implying that the structural transformation occurred after adding methanol to dry ethanol. In contrast, the PXRD patterns of **Zn-CP** after methanol sensing in dry *n*-propanol and dry *n*-butanol were well fitted with the PXRD pattern of as-synthesized **Zn-CP**, indicating that the framework of **Zn-CP** was still maintained after methanol sensing in dry *n*-propanol and dry *n*-butanol (Fig. S20†).

4 Conclusions

The simple synthetic method for **Zn-CP** can be developed using the sonochemical method. **Zn-CP** exhibits a reversible structural transformation to **Zn-CP-II**, with color change induced by thermal and methanol-mediated dehydration and rehydration processes. The luminescence properties of **Zn-CP** and **Zn-CP-II** show weak emission intensities in solid-state but strong emission intensities in suspension with high polar solvents. **Zn-CP** and **Zn-CP-II** contain an ESIPT-sensitive H_4dhtp linker, which not only enhances the interaction between solvent molecules and the frameworks but also facilitates electron transfer *via*

uncoordinated hydroxyl groups in the frameworks. These probes can be used to detect trace amounts of water in dry methanol and dry ethanol. The results show high selectivity, wide linear ranges with good linear relationships, and low LODs. In addition, they can be used for methanol detection in various dry alcohol suspensions, which turn-on luminescence intensity. This work has established a promising model for detecting trace water and methanol in dry organic solvents.

Conflicts of interest

There are no conflicts to declare.

Acknowledgements

Funding for this work was provided by National Research Council of Thailand (NRCT) with Grant No. N41A640144, Material Chemistry Research Center, Research and Graduate Studies, Khon Kaen University. J. S. was financially supported by the Development and Promotion of Science and Technology Talents Project (DPST).

References

1 W. L. Leong and J. J. Vittal, *Chem. Rev.*, 2011, **111**, 688–764.
2 X. Zhang, W. Wang, Z. Hu, G. Wang and K. Uvdal, *Coord. Chem. Rev.*, 2015, **284**, 206–235.
3 W. Xu, K. B. Thapa, Q. Ju, Z. Fang and W. Huang, *Coord. Chem. Rev.*, 2018, **373**, 199–232.
4 N. Stock and S. Biswas, *Chem. Rev.*, 2012, **112**, 933–969.
5 A. V. Desai, S. Sharma, S. Let and S. K. Ghosh, *Coord. Chem. Rev.*, 2019, **395**, 146–192.
6 A. Halder, B. Bhattacharya, F. Haque and D. Ghoshal, *Cryst. Growth Des.*, 2017, **17**, 6613–6624.
7 M. Arıcı, O. Z. Yeşilel and M. Taş, *Dalton Trans.*, 2015, **44**, 1627–1635.
8 J. Suebphanpho, S. Wannapaiboon, S. Youngme and J. Boonmak, *Cryst. Growth Des.*, 2020, **20**, 7439–7449.
9 F. Klongdee, S. Leelasubcharoen, S. Youngme and J. Boonmak, *RSC Adv.*, 2021, **11**, 12218–12226.
10 S. Tunsrichon, S. Youngme and J. Boonmak, *Inorg. Chem.*, 2021, **60**, 18242–18250.
11 S. M. Mobin, A. K. Srivastava, P. Mathur and G. K. Lahiri, *Dalton Trans.*, 2010, **39**, 1447–1449.
12 W.-W. Dong, J. Zhao and L. Xu, *Cryst. Growth Des.*, 2008, **8**, 2882–2886.
13 X. Cui, A. N. Khlobystov, X. Chen, D. H. Marsh, A. J. Blake, W. Lewis, N. R. Champness, C. J. Roberts and M. Schröder, *Chem.–Eur. J.*, 2009, **15**, 8861–8873.
14 V. A. Friese and D. G. Kurth, *Coord. Chem. Rev.*, 2008, **252**, 199–211.
15 J. Liu, Y.-X. Tan and J. Zhang, *Cryst. Growth Des.*, 2012, **12**, 5164–5168.
16 J. Li, P. Du, J. Chen, S. Huo, Z. Han, Y. Deng, Y. Chen and X. Lu, *Anal. Chem.*, 2020, **92**, 8974–8982.
17 S.-Y. Zhu and B. Yan, *Ind. Eng. Chem. Res.*, 2018, **57**, 16564–16571.
18 S. K. Sachan and G. Anantharaman, *Inorg. Chem.*, 2022, **61**, 18340–18345.
19 Y. Zhou, D. Zhang, W. Xing, J. Cuan, Y. Hu, Y. Cao and N. Gan, *Anal. Chem.*, 2019, **91**, 4845–4851.
20 H.-Q. Yin, J.-C. Yang and X.-B. Yin, *Anal. Chem.*, 2017, **89**, 13434–13440.
21 S.-Y. Li, X. Yan, J. Lei, W.-J. Ji, S.-C. Fan, P. Zhang and Q.-G. Zhai, *ACS Appl. Mater. Interfaces*, 2022, **14**, 55997–56006.
22 J. Othong, J. Boonmak, F. Kielar and S. Youngme, *ACS Appl. Mater. Interfaces*, 2020, **12**, 41776–41784.
23 T. Wiwasuku, J. Suebphanpho, S. Ittisanronnachai, V. Promarak, J. Boonmak and S. Youngme, *RSC Adv.*, 2023, **13**, 18138–18144.
24 B. Bhattacharya, A. Halder, L. Paul, S. Chakrabarti and D. Ghoshal, *Chem.–Eur. J.*, 2016, **22**, 14998–15005.
25 R. R. Fonseca, R. D. Gaspar, I. M. Raimundo Jr and P. P. Luz, *J. Rare Earths*, 2019, **37**, 225–231.
26 M. Latha, R. Aruna-Devi, N. Bogireddy, S. E. Rios, W. Mochan, J. Castrellon-Uribe and V. Agarwal, *RSC Adv.*, 2020, **10**, 22522–22532.
27 Z. Jin, H. He, H. Zhao, T. Borjigin, F. Sun, D. Zhang and G. Zhu, *Dalton trans.*, 2013, **42**, 13335–13338.
28 T. Wiwasuku, J. Othong, J. Boonmak, V. Ervithayasuporn and S. Youngme, *Dalton trans.*, 2020, **49**, 10240–10249.
29 A. C. Sedgwick, L. Wu, H.-H. Han, S. D. Bull, X.-P. He, T. D. James, J. L. Sessler, B. Z. Tang, H. Tian and J. Yoon, *Chem. Soc. Rev.*, 2018, **47**, 8842–8880.
30 A. D. Pournara, A. Douvali, S. Diamantis, G. S. Papaefstathiou, A. G. Hatzidimitriou, S. Kaziannis, C. Kosmidis, T. Lazarides and M. J. Manos, *Polyhedron*, 2018, **151**, 401–406.
31 V. Trannoy, N. Guillou, C. Livage, C. Roch-Marchal, M. Haouas, A. Léaustic, C. Allain, G. Clavier, P. Yu and T. Devic, *Inorg. Chem.*, 2019, **58**, 6918–6926.
32 K. Jayaramulu, P. Kanoo, S. J. George and T. K. Maji, *Chem. Commun.*, 2010, **46**, 7906–7908.
33 A. Halder, A. Maiti, S. Dinda, B. Bhattacharya and D. Ghoshal, *Cryst. Growth Des.*, 2021, **21**, 6110–6118.
34 L. Zhang, J. Chen, Y. Ling and Z. Chen, *Chem. Lett.*, 2014, **43**, 997–998.
35 R. Díaz-Torres and S. Alvarez, *Dalton trans.*, 2011, **40**, 10742–10750.
36 M. J. Kamlet, J. L. M. Abboud, M. H. Abraham and R. Taft, *J. Org. Chem.*, 1983, **48**, 2877–2887.
37 G. Mehlana, G. Ramon and S. A. Bourne, *CrystEngComm*, 2013, **15**, 9521–9529.
38 J. Heine and K. Müller-Buschbaum, *Chem. Soc. Rev.*, 2013, **42**, 9232–9242.
39 N. Barman, D. Singha and K. Sahu, *J. Phys. Chem. A*, 2013, **117**, 3945–3953.
40 P. Alam, C. Climent, P. Alemany and I. R. Laskar, *J. Photochem. Photobiol., C*, 2019, **41**, 100317.
41 Z. He, C. Ke and B. Z. Tang, *Acs Omega*, 2018, **3**, 3267–3277.
42 V. S. Padalkar and S. Seki, *Chem. Soc. Rev.*, 2016, **45**, 169–202.
43 L. Dun, B. Zhang, J. Wang, H. Wang, X. Chen and C. Li, *Cryst.*, 2020, **10**, 1105.

44 X. Liu, Y. Wang, Y. Wang, Y. Tao, X. Fei, J. Tian and Y. Hou, *Photochem. Photobiol.*, 2021, **20**, 1183–1194.
45 X. Meng, L. Song, H. Han, J. Zhao and D. Zheng, *Spectrochim. Acta, Part A*, 2022, **265**, 120383.
46 H. Li, W. Han, R. Lv, A. Zhai, X.-L. Li, W. Gu and X. Liu, *Anal. Chem.*, 2019, **91**, 2148–2154.
47 P. Huang, Y. Liu, A. Karmakar, Q. Yang, J. Li, F.-Y. Wu and K.-Y. Deng, *Dalton trans.*, 2021, **50**, 6901–6912.